Oceanologia (2020) 62, 12—22

Available online at www.sciencedirect.com

ScienceDirect

journal homepage: www.journals.elsevier.com/oceanologia/

ORIGINAL RESEARCH ARTICLE

Grain-size characteristics and net transport patterns of surficial sediments in the Zhejiang nearshore area, East China Sea

Juan Liang [a,b,*], **Jian Liu** [c,d], **Gang Xu** [c,d], **Bin Chen** [c,d]

[a] *School of Earth Sciences, China University of Geosciences, Wuhan, China*
[b] *School of Marine Science and Technology, Zhejiang Ocean University, Zhoushan, China*
[c] *Key Laboratory of Marine Hydrocarbon Resources and Environmental Geology, Ministry of Land and Resources, Qingdao, China*
[d] *Qingdao Institute of Marine Geology, Qingdao, China*

Received 11 January 2019; accepted 20 June 2019
Available online 10 July 2019

KEYWORDS
Grain-size trend analysis;
Sediment transport;
Sedimentary rate;
Zhejiang nearshore area

Summary Spatial variations in grain-size parameters can reflect sediment transport patterns and depositional dynamic environments. Therefore, 616 surficial sediment samples taken from the Zhejiang nearshore area in the East China Sea were analyzed to better understand the net sediment transport pattern in this region. The study area is generally dominated by clayey silt and has relatively coarse mud sediment in the southeast. The sorting coefficient of surface sediment is higher than 1.4, and sediment is poorly sorted throughout the study area. The skewness has a strong correlation with the mean grain-size diameter. The net sediment transport pathways obtained by the grain-size trend analysis indicate several distinct characteristics of the surficial sediment transport. The sediment is transported southward under the action of the stronger southward Zhejiang—Fujian Coastal Current (ZMCC) in winter in the upper part of the nearshore area. Influenced by the obstruction of the Taiwan Warm Current (TWC) and the tidal current, surficial sediment transport vectors display two areas of grain-size trend convergence and indicate the net deposition environment has a high sedimentation rate. However, the transport is mainly toward the north under the control of the prevailing northward ZMCC and the strong TWC in the summer. The sedimentary rate is closely related to the processes of the sediment transport. On the one hand, sediment transportation affects the depositional rate in a different

* Corresponding author at: School of Marine Science and Technology, Zhejiang Ocean University, 1 Haida South Road, Lincheng Changzhi Island, Zhoushan, Zhejiang, 316022, China. Tel.: +86 580 8186297.
E-mail address: ljzjou@163.com (J. Liang).

Peer review under the responsibility of Institute of Oceanology of the Polish Academy of Sciences.

Production and hosting by Elsevier

https://doi.org/10.1016/j.oceano.2019.06.002

environment. On the other hand, the modern sedimentary rate can reflect indirectly the sediment source and sediment transportation.

1. Introduction

The spatial variations in grain-size parameters are the natural result of the comprehensive effect of sedimentary dynamics processes in the marine environment. Grain-size parameters can intensively reflect local sedimentary environments, such as hydrodynamic conditions, sediment transport, subsidence, and redistribution processes (Folk, 1966; Passega, 1964; Pejrup, 1988). In particular, abundant information about sediment transport is contained in the sediment grain-size data. Therefore, grain-size analysis is extensively applied to distinguish sediment types, recover sediment mechanisms, and discuss sediment environmental evolution (Asselman, 1999; Cartier and Héquette, 2015; Ma et al., 2014; Pedreros et al., 1996; Rosenberger et al., 2016; Roux, 1994). Many geoscientists are trying to identify sedimentary transport directions according to the spatial variation trends in grain-size parameters. The spatial difference in grain-size parameters is defined as the grain size trends analysis and could be regarded as the results of sediment transport and accumulation (McCave, 1978). Three grain-size parameters (mean size, sorting, and skewness) were utilized to develop a one-dimensional trend model, which could identify the net surficial sediment transport pathways (McLaren, 1981; McLaren and Bowles, 1985). Based on an in-depth study of the McLaren model, a two-dimensional trend method was developed to define net sediment transport patterns: the Grain-Size Trend Analysis (Gao, 1996; Gao and Collins, 1991). The results showed that this pattern could mainly reflect actual sediment transport in areas like estuaries, coasts, and continental shelves (Balsinha et al., 2014; Cheng et al., 2004; Yamashita et al., 2018; Zhang et al., 2013).

The East China Sea (ECS) is a marginal sea with a wide, flat continental shelf in the western Pacific Ocean, which is surrounded by the continent of Asia, China's Taiwan Island, the Korean peninsula, the Kyushu of Japan, and Ryukyu Island. The East China Sea Continental Shelf (ECSCS) is one of the best examples of a river-dominated ocean margin, and its sediment mainly comes from the continental river in surrounding areas. The Yangtze River has long been considered the dominant contributor to the inner-shelf mud area in the ECSCS, which is mainly derived from finer suspended sediments and transported southward by the Zhejiang-Fujian Coastal Current (ZMCC) (Guo et al., 2003; Milliman and Meade, 1983). Researchers have carried out many studies considering sedimentation along the ECSCS, obtaining many beneficial findings. Studies have shown that nearly 47% of the Yangtze River-derived sediment has accumulated in the ECSCS, of which approximately 32% has been deposited in the inner shelf along the Zhejiang—Fujian coasts (Dai et al., 2016; Liu et al., 2007; Saito et al., 2001). Due to the continuous input of the terrigenous and sea sediments, the basic distribution pattern of surface sediments in the ECSCS indicated fine-grained sediments in the nearshore shallow sea and middle continental shelf areas, with coarse sediments in the outer continental shelf area (Li et al., 2012). Moreover, by using ^{210}Pb and ^{137}Cs dating methods, studies on centennial deposition rates indicated that the modern sedimentation rate in the coastal area was higher than that offshore (Su and Huh, 2002; Xu et al., 2012). Ultimately, the mud areas are gradually formed and become depositional centers for the modern continental shelf in the ECS (Liu et al., 2007; Xu et al., 2016).

Many previous studies have investigated the relationship between the sediment distribution in the ECSCS and the corresponding ocean dynamical environment. Some researchers have proposed that the position and deposition rate of the muddy deposits in the continental shelf depend on the sediment supply and the transport ability of the marine dynamics (McKee et al., 1983; Xu et al., 2016). The control of eddy dynamics in the region plays an important role for the formation of mud areas (Hu, 1984). A numerical simulation was applied to analyze the mechanisms that control upwelling on the mud sediment, and it is found that the upwelling can increase the depositional process of fine-particle sediments (Qu and Hu, 1993; Zhang et al., 2011). The sediment transport in the ECSCS is strongly influenced by the Taiwan Warm Current (TWC) and the coastal current in the ECS. Moreover, the coastal currents in the ECS are necessary for the formation of the coastal mud area in the inner shelf (Liu et al., 2007; Xu et al., 2009). Based on the sedimentary velocity and granularity of the sediment, the possible generating process of mud areas was better elaborated (Demaster et al., 1985). After analyzing the seasonal variation of suspension sources and vortex dynamics in the mud area to the north of the ECSCS, the results showed that there are obvious seasonal differences in the sedimentation dynamics of the mud area (Wang et al., 2014). According to the in situ observations of the ocean temperature, salinity, flow, and suspension turbidity, the results indicate that the major force driving the sediment to suspend and transport is the tidal current, and the sediment supplied by the Yangtze River is transported southwards along the coast (Sternberg et al., 1985). Satellite remote sensing image data and numerical simulations were also used to study the seasonal differences of the sedimentary processes of the mud areas in the ECSCS, and the results indicated that the inner mechanism has a close relationship with the seasonal variations of the supply from river sediments, marine dynamic factors, and the ocean current system (Moon et al., 2009; Yanagi et al., 1996; Yuan et al., 2008). However, previous studies mostly focused on the relationship between the sedimentation processes with a single influencing factor, especially when sediment transport was analyzed. These previous studies have primarily emphasized the influence of the marine environment on the sediment transport pathway, providing

somewhat superficial insight into the effects of sediment transport on the sedimentary environment. Therefore, the objectives of this paper are to (1) clarify the changes in the surficial sediment distributions in the Zhejiang nearshore area; (2) illuminate the sediment transport patterns by grain-size trend analysis; and (3) expound on explicating the interaction between surficial sediment transport patterns and the marine deposition environment. In addition, combining the results with long-term accumulation rates based on ^{210}Pb dating helps improve understanding of erosion and deposition in the nearshore mud area.

2. Regional setting

This study area lies in the southwest of the ECSCS between 28°N–31°N and 121°30′E–123°E (Fig. 1). The northern coast of the Zhejiang Province is located in the southern wing of the Yangtze River Delta and Qiantang River Estuary Plain, while southern regions are the low hilly shoreline of volcanic rock (Fig. 2). The terrain of the nearshore area slopes downward from northwest to southeast and until plunges down to the East China Sea, with some mountains becoming islands. The Zhoushan Archipelago, adjacent to the Yangtze Estuary and Hangzhou Bay, is northwest of the study area. Islands are scattered in the Zhoushan sea area, where fjords are plentiful between the islands and the water depth is greater. There are large and small mountainous river dispersal systems, such as the Qiantang River. Large amounts of sediment from these rivers are transported to the nearshore area, with a part of sediment originating from the Yangtze Estuary. The twists and turns of the nearshore area create a coastline of more than 6000 km, distributed with bays like the Hangzhou, Xiangshan, Sanmen, Taizhou, and Yueqing Bays. The coastal types of Zhejiang Province could be generalized into the muddy (about 50% of total length), bedrock (40%), and sand coast (4%). Under the influence of the hydrodynamic condition and sediment source, these coasts have obvious seasonal variations: erosion in summer and deposition in winter.

The climate factors, such as heat, temperature, precipitation, and evapotranspiration, vary obviously with seasonal and latitudinal changes. The annual temperature increases from the north to the south, varying from 16 to 21°C. The annual rainfall is between 900 and 1300 mm, with a tendency to be higher in the south and lower in the north in coastal regions. The main tidal characteristics are mixed semidiurnal tides with medium tide ranges and high current velocities. The flood currents come from the outer shelf and flow toward the nearshore area, while the ebb currents have the opposite behavior. Moreover, this area is often threatened by typhoons and strong tropical storms. Surge waves are more frequent

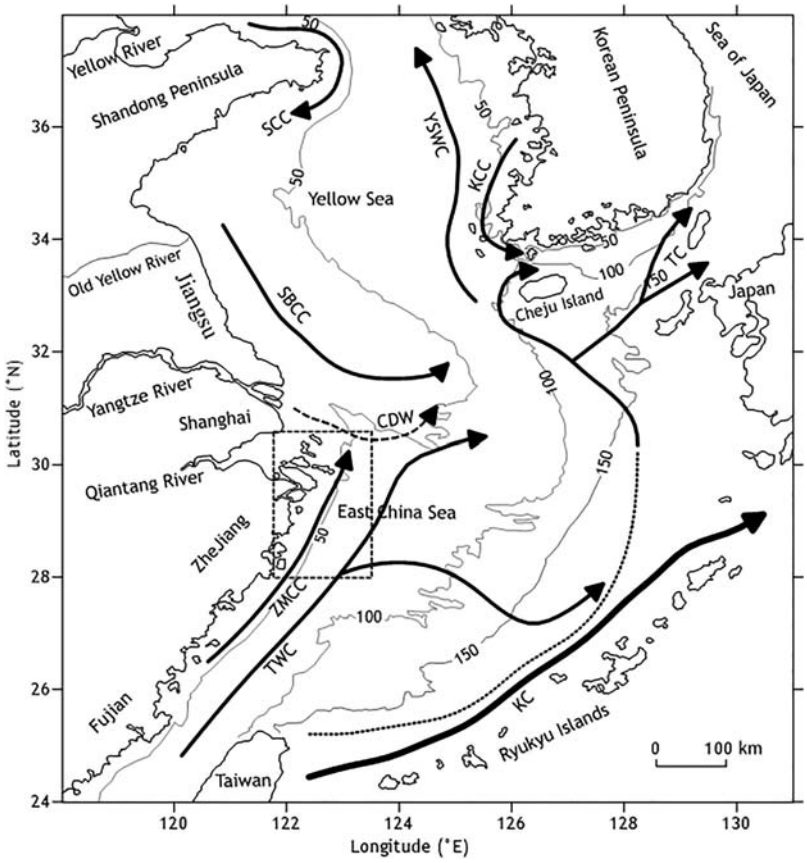

Figure 1 Schematic map of the bathymetry and regional circulation pattern in the ECSCS and adjacent areas during summertime (modified after Liu et al., 2010). Water depth in meters. The dashed square indicates the study area. SSCC, South Shandong Coastal Current; YSWC, Yellow Sea Warm Current; KCC, Korean Coastal Current; NJCC, North Jiangsu Coastal Current; CDW, Changjiang (Yangtze River) Diluted Water; ZMCC, Zhejiang–Fujian Coastal Current; TWC, Taiwan Warm Current; KC, Kuroshio Current; TC, Tsushima Current.

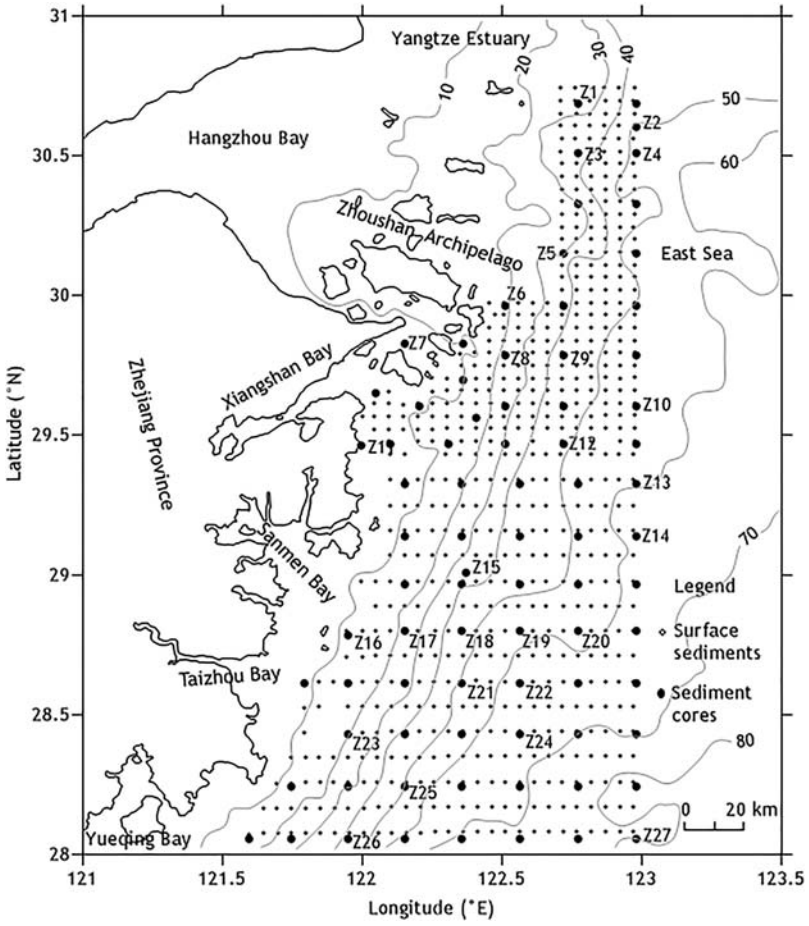

Figure 2 Location of the surface sediment and columnar core samples in the Zhejiang nearshore area. Water depth in meters. (The numbered core samples were chosen for ^{210}Pb and ^{137}Cs experiments.)

than wind waves affected by the southeasterly winds (Liu et al., 2006; Zhang et al., 2014).

The general current circulation system in the study area is dominated by the KC, TWC, and coastal current (Fig. 1). The KC, which originates from the north equatorial warm current, intrudes onto the ECSCS on the large scale and flows northeast along the edge of the continental shelf (Andres et al., 2008; Li et al., 2013; Zheng and Huang, 1993). The TWC is parallel to the KC and is characterized by a high temperature, high salinity, and low turbidity, and it flows northward all year round along the coast, with stronger currents in the summer than in the winter (Fang et al., 1991). The ZMCC is formed in a seashore environment and flows northward in the summer and southward in the winter due to monsoons (Su, 2001). The circulation patterns mentioned above control the sediment transport processes and affect the sediment framework in the study area.

3. Material and methods

3.1. Field sampling

616 surficial sediment samples were collected with box core from the Zhejiang nearshore area on board of the R/V *Yezhizheng* in June 2013 (Fig. 2). The positions of the samples were determined using a differential GPS system. The samples were about 3 cm thick and were taken from the superficial layer of each box core, and 10 g samples were chosen for the grain-size analytical experiment. Meanwhile, 80 columnar cores (2.2—3.5 m long each) were collected with a vibrocorer. According to the geological and topographic features of the study area, 27 columnar cores were chosen for ^{210}Pb and ^{137}Cs experiments.

3.2. Grain size experiment

The samples were pretreated with 10% H_2O_2 and 0.1 N HCl to remove organic matter and biogenic carbonate, respectively. Then, the samples were dispersed with 0.5% $(NaPO_3)_6$ and subsequent ultrasonic dispersion. The grain size was measured with a Malvern Mastersizer 2000 Laser particle size analyzer (Malvern Instruments Ltd., UK), with a measuring range from 0.02 to 2000 μm, a particle resolution of 0.01 ϕ, and relative error of <2%. Three main grain-size parameters, including mean diameter (μ), sorting coefficient (σ), and skewness (Sk), were calculated using the statistic moment method (McManus, 1988):

$$\mu = \sum_{1}^{n} P_i S_i, \quad (1)$$

$$\sigma = \left[\sum_{1}^{n} P_i(S_i-\mu)^2\right]^{1/2}, \quad (2)$$

$$Sk = \left[\sum_{1}^{n} P_i(S_i-\mu)^3\right]^{1/3}, \quad (3)$$

where S_i is the size class, P_i is the percentage of size S_i (in ϕ units), and n is the total number of size classes. The Shepard classification scheme (Shepard, 1954) was adopted in this study to describe the sediment types of surficial sediment samples.

3.3. Columnar cores and ^{201}Pb dating

The subsamples of 27 columnar cores for ^{210}Pb, ^{226}Ra, and ^{137}Cs analysis were selected at 5–10 cm intervals to calculate sediment accumulation rates for the sample sites. ^{210}Pb activities were determined by a BE3830 gamma-ray spectrometer (CANBERRA Ltd., USA) following a standard operation procedure (Xia et al., 2011), and the uncertainties associated with sample measurements were typically less than 10%. Supported ^{210}Pb activities were assumed to be equal to the measured ^{226}Ra activities, and excess ^{210}Pb activities were calculated by subtracting the supported ^{210}Pb activities from the total ^{210}Pb activities measured (Pfitzner et al., 2004). The influence of grain-size variations on the ^{210}Pb activities was eliminated by normalizing the ^{210}Pb activities to the corresponding clay (<4 μm) content of each sample (Palinkas et al., 2006). The sediment accumulation rates were calculated by means of a Constant Initial Concentration model (Oldfield et al., 1978). Analyses of grain size and ^{210}Pb dating experiments were carried out at the Center of Testing, Qingdao Institute of Marine Geology, China Geological Survey.

3.4. Grain-size trend analysis

Grain-size trends were calculated in this study by operating the two-dimensional model that can describe net sediment transport patterns (Gao and Collins, 1994). This method is based on the assumption that the trend used for the analysis has a significantly higher probability of occurrence in the direction of net transport than in any other directions (Gao, 1996). It tries to identify the possible net transport paths by comparing two neighboring sampling sites. By employing the three most frequently used grain-size parameters (μ, σ, and Sk), the most appropriate grain-size trends for trend analysis can be found (Gao and Collins, 1994). Then, by comparing the three grain-size parameters between the two nearest neighboring stations within a characteristic distance, a dimensionless trend vector is defined. The vector has a unit length and points from the station with the higher sorting coefficient toward that with the lower sorting value. Each of the two neighboring stations are compared in a grid of surficial sediment samples, and all of the grain-size trend vectors are generated. A single resultant vector is produced after summing the identified trend vector at each sampling station and its neighboring stations. This resultant vector represents the tendency of the sediment transport at the station. Finally, a smoothing operation is performed to remove background noise by averaging the resultant vector at any sampling station and the resultant vectors of its neighboring stations to produce a residual vector. The transport vector maps can successfully reflect the net sediment transport trend via this sequence of steps.

4. Results and discussion

4.1. Sediment compositions and distributions patterns

Surface sediments were classified and plotted in a ternary diagram of sand (>0.063 mm), silt (0.004–0.063 mm), and clay (<0.004 mm) contents (Fig. 3). Five primary sediment types occur in the Zhejiang nearshore area: clayey silt (YT), sand-silt-clay (STY), silty sand (TS), silt (T), and fine sand (FS) (Fig. 4). YT is the dominant sediment type (74% of all 616 surficial sediment samples) and is primarily deposited in the center of the nearshore area with a NE–SW banding distribution, which is also known as the mud area in shallow sea water. T (2%) is scattered along the coastline and mainly originates from the Yangtze River and some mountain rivers. From the center to the eastern deep water more than 50 m, STY (16%), TS (6%), and FS (2%) gradually become present, and sediments become gradually coarser in grain size. Overall, there are coarse-fine-coarse gradations in the grain sizes of the sediments from the nearshore to the offshore.

The distributions of size fraction components (sand, silt, and clay) correspond well with those of the surficial sediment types (Fig. 4). The sand component is distributed much less widely, mainly in the offshore area, compared with the silt and clay in the study area (Fig. 5a). The high content of the sand component benefits from the contributions of residual sand sediment from the ECSCS (Niino and Emery, 1961; Shen, 1986). The silt component is distributed in the western nearshore area and presents a zonal distribution, ranging from 50% to 70%. A relatively high silt component appears near the Zhejiang coast, which is abundant in terrigenous sediment supply transported by the ZMCC and some mountain rivers (Fig. 5b). The clay component (average 28%) is generally distributed in the middle of the Zhejiang nearshore

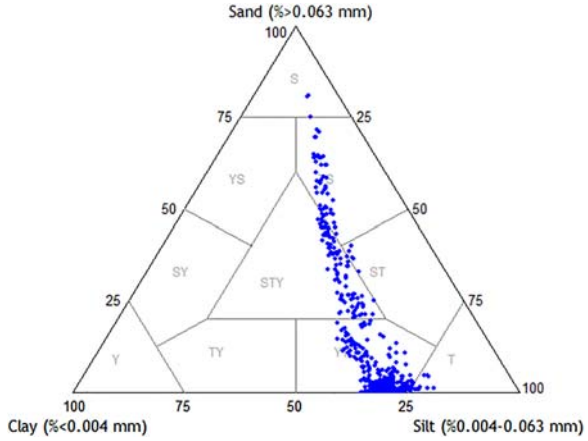

Figure 3 Ternary diagram of sand/silt/clay proportions of samples in the Zhejiang nearshore area (S, sand; T, silt; Y, clay; YS, clayey sand; TS, silty sand; SY, sandy clay; S-T-Y, sand-silt-clay; ST, sandy silt; TY, silty clay; YT, clayey silt).

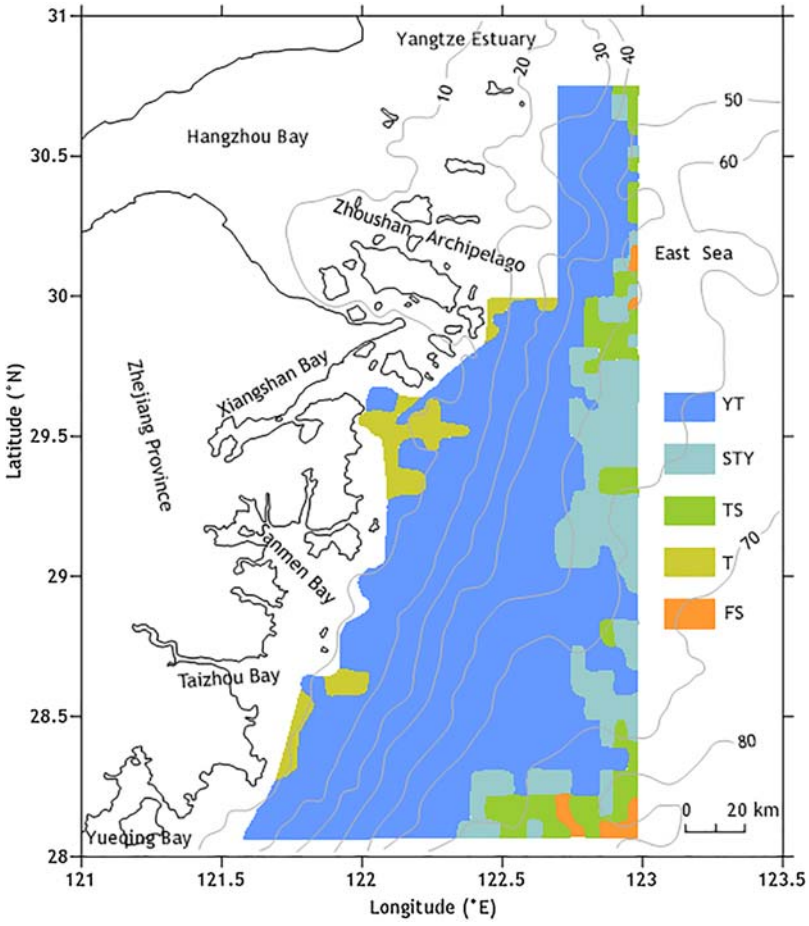

Figure 4 Spatial distribution of the surficial sediment types in the Zhejiang nearshore area. Water depth in meters.

area, known as the mud area in the inner shelf (Fig. 5c) (Liu et al., 2007; Xu et al., 2016). The clay content gradually diminishes toward the edges of the center area.

4.2. Log-ratio and correlation analysis of grain-size parameters

The spatial distribution of the mean diameter of the surface sediments shows a clear coarse-fine-coarse trend from the shallow water to the deep water of the nearshore area (Fig. 6a). The mean diameters of the surface sediments vary generally from 2.9 ϕ to 7.5 ϕ and reach their peaks at the center region, which is the mud area in the nearshore area. The surface sediment becomes coarser with increasing distance from the nearshore region. Finally, the coarsest sediments (<3 ϕ) occur in the southeastern regions of the nearshore area. The sorting coefficients of surface sediment are generally larger than 1.3, indicating relatively poor

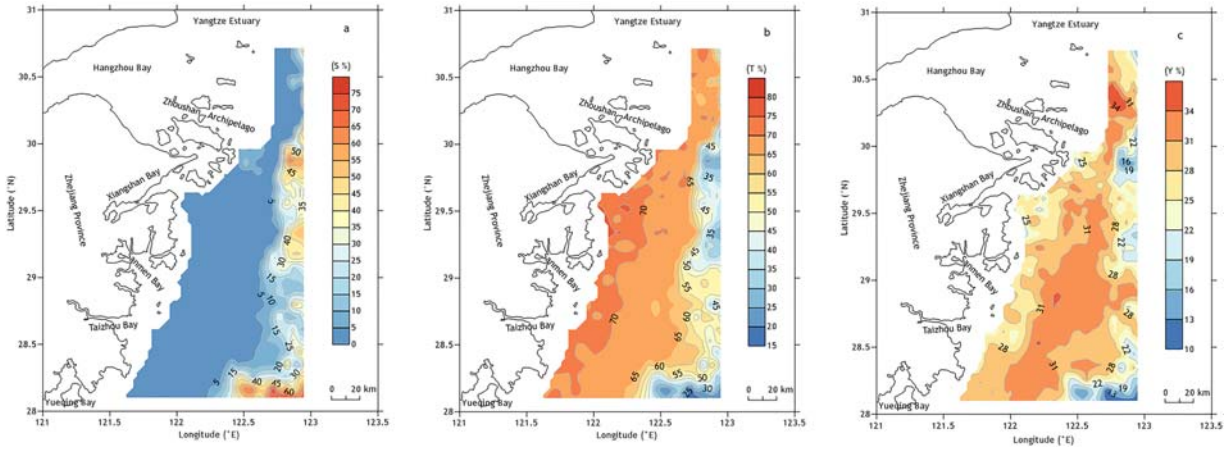

Figure 5 Spatial distributions of the contents of the sand (a), silt (b), and clay (c) in the Zhejiang nearshore area.

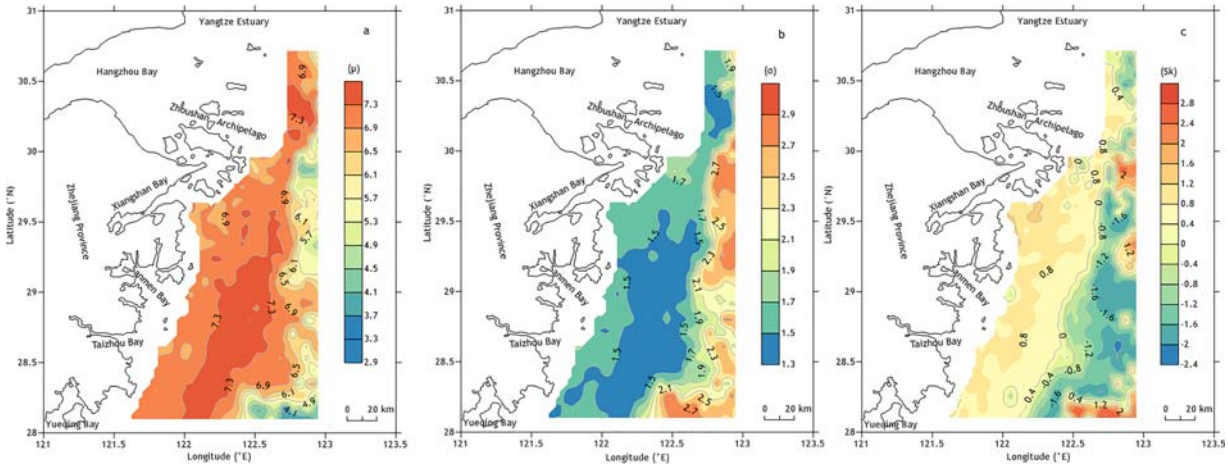

Figure 6 Spatial distributions of the mean diameter of the surface sediment (a), the sorting coefficient (b), and the skewness (c) in the Zhejiang nearshore area.

sorting in the study area (Fig. 6b). However, the sorting is relatively better in the southeastern regions with the distribution of the coarser sediments. The spatial distribution of the sorting coefficient is similar to that of the mean size. Size distributions in the study area are almost symmetrical, with values of skewness varying from −2.4 to 2.8 (Fig. 6c). Higher values are generally located at the two sides of the center mud area. And lower values occur over the central eastern parts. The main factors affecting the spatial distribution of grain-size parameters are sediment sources and characteristics, hydrodynamic conditions, and topography features.

The correlativity between the sorting coefficient, skewness, and mean diameter is presented in Fig. 7. As the mean diameter decreases from 3 ϕ to 6 ϕ, the sorting coefficient of surface sediments keeps the high value from 2.4 to 2.8 and generally does not change obviously (Fig. 7a). However, with the further decrease in mean diameter from 6 ϕ to 8 ϕ, it seems a sorting improves. The skewness has a strong correlation with the mean grain diameter. For surface sediments with a median diameter of 3–5.5 ϕ, their skewnesses are positively skewed (Fig. 7b). When the median grain diameter is higher than 6 ϕ, the sediment size distributions become more negatively skewed, with part cases of positive skewness. Overall, it shows that the skewness changes from positive to symmetrical and then to negative with the decrease in median grain diameter. These tendencies of

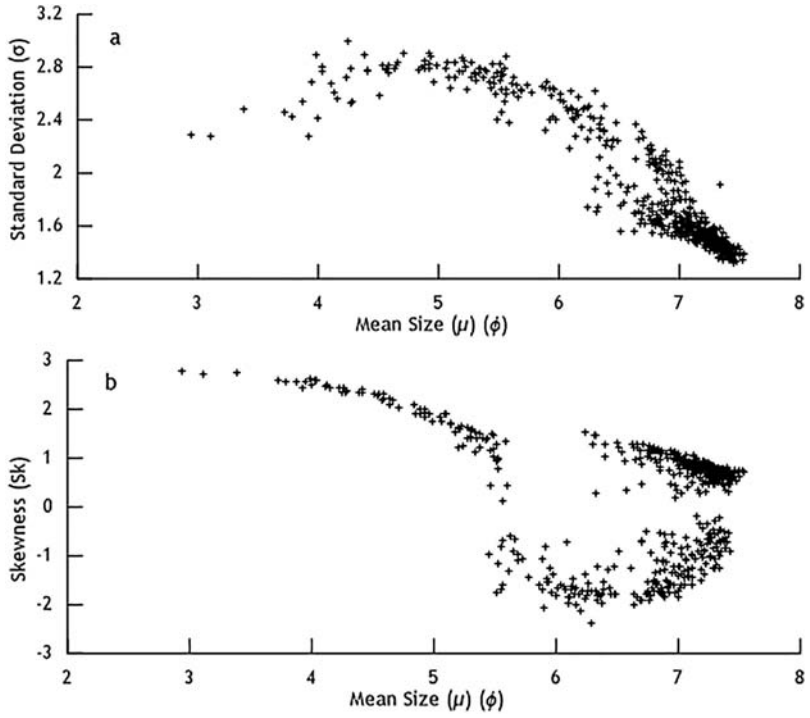

Figure 7 Relationship between mean size (ϕ) and sorting (a), and mean size (ϕ) and skewness (b) in the Zhejiang nearshore area.

the skewness change are probably related to the accumulation and erosion of the sedimentary environment in the study area.

4.3. Net sediment transport pathways

The net sediment transport patterns, obtained by the grain-size trend analysis, reveal several distinct characteristics in the Zhejiang nearshore area (Fig. 8). The arrows indicate the direction of sediment transport. The lengths of the resultant vectors do not represent the intensity of sediment transport but rather the significance of transport trends (Gao and Collins, 1994). The surficial sediment transport seems relatively complicated due to the comprehensive influence of the topographical conditions, hydrodynamic characteristics, and sediment sources in the study area.

In the northeastern Zhoushan Archipelago area, the sediment is clearly transported southward due to the stronger southward ZMCC prevailing in winter. Meanwhile, both the velocity and duration of the flood-tide are larger than those of the ebb-tide under the influence of the funnel shape topography of Hangzhou Bay. This can be seen from the distribution trends of the bathymetric contour (Fig. 2). Affected by the transportation function of the tidal current flowing from the outer shelf to Hangzhou Bay, the accumulation of sediment supplied mainly from the Yangtze River occurs in this region. Transport trends in this region also show that there is a depositional environment with a convergence of the transport vectors. Likewise, in the southern Zhoushan Archipelago area, the sediments are transported southeastward through some fjords between these islands. There is also a significant convergence, counter-balanced by the TWC and the coastward flood current.

To the south of Sanmen Bay, the residual vector pattern shows northeastward transport along the coast because the surficial sediment transport is a comprehensive and long-term system process. The ZMCC is dominant northward in the summer (Su, 2001). Moreover, the powerful TWC flows northward through the Taiwan Strait, preventing the sediments transported by the ZMCC from continuing seaward transport. The seasonality of these currents helps to determine the paths of transport. Therefore, the sediments are transported toward the northeast along the coast in this region. However, it can clearly be seen that the vectors display a northwestern trend in the eastern part of this area. Surficial sediment transport is controlled by the combined effects of the TWC and a tidal current flowing from the sea, which results in the surface sediment being transported northwestward. Thus, transport trends in this region also indicate a smaller convergence.

In addition, it is worth mentioning that the nearshore upwelling plays a significant role in intensifying the sediment transportation pattern toward the coast in some periods. Some studies have shown that the sea-bottom upwelling can prompt the fine particles from the outer shelf to be transported and deposited toward the coast (Hu, 1984; Qu and Hu, 1993; Wang et al., 2014). Under the control of the sediment transport process mentioned above, the sediments from the Yangtze River and other sources are accumulated along the coast in the study area, with enormous thickness deposition (referred to as mud belt deposit) on the inner shelf of the ECS (Liu et al., 2014).

4.4. Spatial distributions of sedimentation rate

The spatial distribution of ^{210}Pb sediment accumulation rates in the study area is shown in Fig. 9. Generally, the sedimentation rate gradually decreases from north to south. The highest rates are seen in the Zhoushan Archipelago area, dominantly varying from 2.4 to 3.9 cm/a, and the lowest are

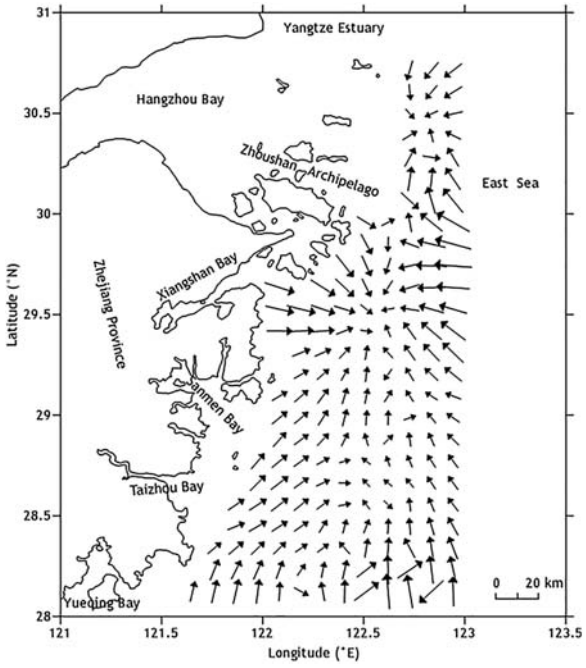

Figure 8 Distribution of residual transport vectors in the Zhejiang nearshore area.

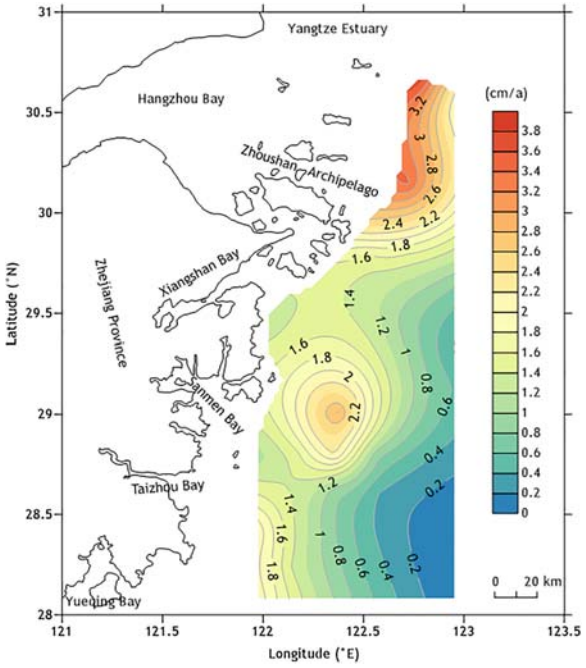

Figure 9 Spatial distribution variation in the modern sedimentary rate in the Zhejiang nearshore area.

seen at the southeastern outer shelf at less than 0.2 cm/a. Then the sedimentation rate declines from nearshore to offshore, both in the northern and southern regions. However, the deposition rate is relatively high (2.8 cm/a) in the central part of the study area and gradually declines from the center to the coast and offshore areas. Some previous studies have shown similar results along the coast of the ECS (Chen et al., 2004; Demaster et al., 1985; Liu et al., 2006; Su and Huh, 2002). Overall, the shoreward shallow area is a high modern sedimentary rate area in water less than 40 m deep (Figs. 9 and 2). From nearshore to offshore, the depositional rate is gradually reduced with increasing water depth. Finally, the sedimentary rate is almost zero with a depth of more than 70 m, which is presumably associated with erosion.

The sediment transport pathway is important because it determines the topography of the nearshore area. However, the sedimentation rate is a key parameter for the evolution of erosion and deposition in marine topography. The spatial distributions of sedimentation rate are closely related to the sediment sources, hydrodynamic conditions, and sediment transport. In the waters adjacent to the Zhoushan Archipelago and Xiangshan Bay, a large amount of sediment from the Yangtze River is transported southward under the control of the ZMCC and deposited rapidly, which leads to high sedimentation rates. Accordingly, the transport trends in the high modern sedimentation rate area also show that there is a depositional environment with the convergence of the transport vectors (Fig. 8).

In the southern area of Sanmen Bay, the TWC prevents the suspended sediment from being further transported to the outer shelf in the ECS. The thick, finer sedimentary layers occur in the nearshore area, which are known as the mud area in the inner shelf. Previous studies have revealed that mud areas are the depositional center during high sea levels since the last deglaciation period (Li et al., 2012; Liu et al., 2007; Xu et al., 2012). When it comes to the sand composition deposited in the southeastern Zhejiang nearshore area, the lowest sedimentation rate appears and approaches zero (Figs. 4 and 9). This is influenced by the residual sand in the middle and outer shelves of the ECS (Wang et al., 2012). The residual sediments belong to the marine sedimentary environment in the last stage of the late Pleistocene and are reformed by modern marine dynamics. Ultimately, a coarser reconstructive deposition called the residual sand is left in place, and the suspended finer sediment is carried by the flood current to the nearshore area (Liu, 1987; Xu et al., 2009).

5. Conclusions

Surface sediments of the Zhejiang nearshore area were analyzed in this study in order to better understand the sediment transport process. Grain-size distributions of the surface sediment show a mud area and the domination of clayey silt. Generally, the mean diameters of the surface sediments display an apparent coarse-fine-coarse trend from the shallow water to the deep water of the nearshore area. However, the sorting coefficient of surface sediments is relatively high, and sediment is poorly sorted over the study area. There is no significant correlation between the sorting coefficient and the medium grain diameter. Nevertheless, the skewness has a strong correlation with the mean grain diameter. Coarse sediment is associated with higher skewness of the corresponding size distribution, while the size distribution of finer sediment shows a relatively lower skewness.

The grain-size trend analysis was employed to ascertain the net surficial sediment transport pattern in the Zhejiang nearshore area. The results reveal that the sediment transport is closely related to the sediment sources, hydrodynamic conditions, and topographical features in the ECSCS. There are several distinct characteristics of the surficial sediment transport. In the northern part of the study area, sediments are transported southward under the action of the stronger southward ZMCC in the winter. Simultaneously being affected by the obstruction of the TWC and the tidal current, surficial sediment transport vectors display two grain-size trend convergences and indicate a high-speed sedimentation environment. Accordingly, there is a high modern sedimentation rate in this region. In the southern part, however, the transport is mainly toward the north under the control of the prevailing northward ZMCC and the strong TWC in summer. The surficial sediment transport trends agree well with the sedimentation rate distribution pattern on the basis of the ^{210}Pb dating data, which implies that the sedimentation rate validates the results of the grain-size trend analysis and makes up for the disadvantages of the grain trend size analysis in predicting erosion and deposition of the topography. The results of this study only represent long-term average sediment transport. Further studies should pay attention to the specific exchange process between surface sediment and suspended sediment.

Acknowledgments

This research was financially supported by the National Basic Research Program of China (Grant No. GZH201200506), the China-ASEAN maritime cooperation fund: Comparative study of Holocene Sedimentary Evolution of the Yangtze River Delta and the Red River Delta. We thank the fieldwork group and laboratory staff of the program for this contribution. This manuscript benefited from comments and suggestions from Prof. Janusz Pempkowiak and two anonymous reviewers.

References

Andres, M., Wimbush, M., Park, J.H., Chang, K.I., Lim, B.H., Watts, D.R., Ichikawa, H., Teague, W.J., 2008. Observations of Kuroshio flow variations in the East China Sea. J. Geophys. Res. 113 (C5) C05013, 14 pp., http://dx.doi.org/10.1029/2007JC004200.

Asselman, N.E.M., 1999. Grain-size trends used to assess the effective discharge for floodplain sedimentation, River Waal, the Netherlands. J. Sediment. Res. A 69 (1), 51—61, http://dx.doi.org/10.2110/jsr.69.51.

Balsinha, M., Fernandes, C., Oliveira, A., Rodrigues, A., Taborda, R., 2014. Sediment transport patterns on the Estremadura Spur continental shelf: insights from grain-size trend analysis. J. Sea Res. 93, 28—32, http://dx.doi.org/10.1016/j.seares.2014.04.001.

Cartier, A., Héquette, A., 2015. Vertical distribution of longshore sediment transport on barred macrotidal beaches, northern France. Cont. Shelf Res. 93, 1—16, http://dx.doi.org/10.1016/j.csr.2014.11.009.

Chen, Z., Saito, Y., Kanai, Y., Wei, T., Li, L., Yao, H., Wang, Z., 2004. Low concentration of heavy metals in the Yangtze estuarine sediments, China: a diluting setting. Estuar. Coast. Shelf Sci. 60 (1), 91—100, http://dx.doi.org/10.1016/j.ecss.2003.11.021.

Cheng, P., Gao, S., Bokuniewicz, H., 2004. Net sediment transport patterns over the Bohai Strait based on grain size trend analysis. Estuar. Coast. Shelf Sci. 60 (2), 203—212, http://dx.doi.org/10.1016/j.ecss.2003.12.009.

Dai, Z., Fagherazzi, S., Mei, X., Gao, J., 2016. Decline in suspended sediment concentration delivered by the Changjiang (Yangtze) River into the East China Sea between 1956 and 2013. Geomorphology 268, 123—132, http://dx.doi.org/10.1016/j.geomorph.2016.06.009.

Demaster, D.J., Mckee, B.A., Nittrouer, C.A., Qian, J., Cheng, G., 1985. Rates of sediment accumulation and particle reworking based on radiochemical measurements from continental shelf deposits in the East China Sea. Cont. Shelf Res. 4 (1), 143—158, http://dx.doi.org/10.1016/0278-4343(85)90026-3.

Fang, G., Zhao, B., Zhu, Y., 1991. Water volume transport through the Taiwan Strait and the continental shelf of the East China Sea measured with current meters. Elsev. Oceanogr. Ser. 54, 345—358, http://dx.doi.org/10.1016/S0422-9894(08)70107-7.

Folk, R.L., 1966. A review of grain-size parameters. Sedimentology 6 (2), 73—93, http://dx.doi.org/10.1111/j.1365-3091.1966.tb01572.x.

Gao, S., 1996. A FORTRAN program for grain-size trend analysis to define net sediment transport pathways. Comput. Geosci. 22 (4), 449—452, http://dx.doi.org/10.1016/0098-3004(95)00100-X.

Gao, S., Collins, M., 1991. A critique of the "McLaren Method" for defining sediment transport paths. J. Sediment. Petrol. 61 (1), 143—146, http://dx.doi.org/10.1306/D42676A9-2B26-11D7-8648000102C1865D.

Gao, S., Collins, M., 1994. Net sediment transport patterns inferred from grain-size trends, based upon definition of "transport vectors" — reply. Sediment. Geol. 90 (1—2), 157—159, http://dx.doi.org/10.1016/0037-0738(94)90023-X.

Guo, Z., Yang, Z., Fan, D., Pan, Y., 2003. Seasonal variation of sedimentation in the Changjiang Estuary mud area. J. Geogr. Sci. 13 (3), 348—354, http://dx.doi.org/10.1007/bf02837510.

Hu, D., 1984. Upwelling and sedimentation dynamics: I. The role of upwelling in sedimentation in the Huanghai Sea and East China Sea — a description of general features. Chin. J. Oceanol. Limnol. 2 (1), 12—19, http://dx.doi.org/10.1007/BF02888388.

Li, J., Wei, H., Zhang, Z., Lu, Y., 2013. A modelling study of interannual variation of Kuroshio intrusion on the shelf of East China Sea. J. Ocean Univ. China 12 (4), 537—548, http://dx.doi.org/10.1007/s11802-013-2203-z.

Li, P., Yang, S.L., Milliman, J.D., Xu, K.H., Qin, W.H., Wu, C.S., Chen, Y.P., Shi, B.W., 2012. Spatial, temporal, and human-induced variations in suspended sediment concentration in the surface waters of the Yangtze Estuary and adjacent coastal areas. Estuar. Coast. 35 (5), 1316—1327, http://dx.doi.org/10.1007/s12237-012-9523-x.

Liu, J., Saito, Y., Kong, X., Wang, H., Xiang, L., Wen, C., Nakashima, R., 2010. Sedimentary record of environmental evolution off the Yangtze River estuary, East China Sea, during the last ~13,000 years, with special reference to the influence of the Yellow River on the Yangtze River delta during the last 600 years. Quaternary Sci. Rev. 29 (17—18), 2424—2438, http://dx.doi.org/10.1016/j.quascirev.2010.06.016.

Liu, J.P., Li, A.C., Xu, K.H., Velozzi, D.M., Yang, Z.S., Milliman, J.D., DeMaster, D.J., 2006. Sedimentary features of the Yangtze River-derived along-shelf clinoform deposit in the East China Sea. Cont. Shelf Res. 26 (17—18), 2141—2156, http://dx.doi.org/10.1016/j.csr.2006.07.013.

Liu, J.P., Xu, K.H., Li, A.C., Milliman, J.D., Velozzi, D.M., Xiao, S.B., Yang, Z.S., 2007. Flux and fate of Yangtze River sediment delivered to the East China Sea. Geomorphology 85 (3—4), 208—224, http://dx.doi.org/10.1016/j.geomorph.2006.03.023.

Liu, S., Shi, X., Fang, X., Dou, Y., Liu, Y., Wang, X., 2014. Spatial and temporal distributions of clay minerals in mud deposits on the inner shelf of the East China Sea: implications for paleoenvironmental changes in the Holocene. Quatern. Int. 349, 270—279, http://dx.doi.org/10.1016/j.quaint.2014.07.016.

Liu, X., 1987. Relict sediments in China continental shelf. Mar. Geol. Quat. Geol. 7 (1), 1—14, http://en.cnki.com.cn/Article_en/CJFDTOTAL-HYDZ198701000.

Ma, X., Yan, J., Fan, F., 2014. Morphology of submarine barchans and sediment transport in barchans fields off the Dongfang coast in Beibu Gulf. Geomorphology 213 (10), 213—224, http://dx.doi.org/10.1016/j.geomorph.2014.01.010.

McCave, I.N., 1978. Grain-size trends and transport along beaches; example from eastern England. Mar. Geol. 28 (1—2), 43—51, http://dx.doi.org/10.1016/0025-3227(78)90092-0.

McKee, B.A., Nittrouer, C.A., Demaster, D.J., 1983. Concepts of sediment deposition and accumulation applied to the continental shelf near the mouth of the Yangtze River. Geology 11 (11), 631—633, http://dx.doi.org/10.1130/0091-7613(1983)11<631:COSDAA>2.0.CO;2.

McLaren, P., 1981. An interpretation of trends in grain size measures. J. Sediment. Res. 51 (2), 0611—0624, http://dx.doi.org/10.1306/212F7CF2-2B24-11D7-8648000102C1865D.

McLaren, P., Bowles, D., 1985. The effects of sediment transport on grain-size distributions. J. Sediment. Res. 55 (4), 0457—0470, http://dx.doi.org/10.1306/212F86FC-2B24-11D7-8648000102C1865D.

McManus, J., 1988. Grain size determination and interpretation. In: Tucker, M. (Ed.), Techniques in Sedimentology. Blackwell, Oxford, 63—85, https://ci.nii.ac.jp/naid/10004029583/en.

Milliman, J.D., Meade, R.H., 1983. World-wide delivery of river sediment to the oceans. J. Geol. 91 (1), 1—21, http://dx.doi.org/10.1086/628741.

Moon, J.-H., Pang, I.-C., Yoon, J.-H., 2009. Response of the Changjiang diluted water around Jeju Island to external forcings: a modeling study of 2002 and 2006. Cont. Shelf Res. 29 (13), 1549—1564, http://dx.doi.org/10.1016/j.csr.2009.04.007.

Niino, H., Emery, K.O., 1961. Sediments of shallow portions of East China Sea and South China Sea. Geol. Soc. Am. Bull. 72 (5), 731—762, http://dx.doi.org/10.1130/0016-7606(1961)72[731:SOSPOE]2.0.CO;2.

Oldfield, F., Appleby, P.G., Battarbee, R.W., 1978. Alternative ^{210}Pb dating: results from the New Guinea Highlands and Lough Erne. Nature 271 (5643), 339—342, http://dx.doi.org/10.1038/271339a0.

Palinkas, C.M., Nittrouer, C.A., Walsh, J.P., 2006. Inner-shelf sedimentation in the Gulf of Papua, New Guinea: a mud-rich shallow shelf setting. J. Coastal Res. 224 (4), 760—772, http://dx.doi.org/10.2112/03-0086.1.

Passega, R., 1964. Grain size representation by CM patterns as a geologic tool. J. Sediment. Res. 34 (4), 830—847, http://dx.doi.org/10.1306/74D711A4-2B21-11D7-8648000102C1865D.

Pedreros, R., Howa, H.L., Michel, D., 1996. Application of grain size trend analysis for the determination of sediment transport pathways in intertidal areas. Mar. Geol. 135 (1—4), 35—49, http://dx.doi.org/10.1016/S0025-3227(96)00042-4.

Pejrup, M., 1988. The triangular diagram used for classification of estuarine sediments: a new approach. In: de Boer, P.L., van Gelder, A., Nio, S.D. (Eds.), Tide-Influenced Sedimentary Environments and Facies. Reidel, Dordrecht, 289—300, http://dx.doi.org/10.1007/978-94-015-7762-5_21.

Pfitzner, J., Brunskill, G., Zagorskis, I., 2004. ^{137}Cs and excess ^{210}Pb deposition patterns in estuarine and marine sediment in the central region of the Great Barrier Reef Lagoon, north-eastern Australia. J. Environ. Radioactiv. 76 (1—2), 81—102, http://dx.doi.org/10.1016/j.jenvrad.2004.03.020.

Qu, T., Hu, D., 1993. Upwelling and sedimentation dynamics II. A simple model. Chin. J. Oceanol. Limnol. 11 (14), 289—384, http://dx.doi.org/10.1007/BF02850633.

Rosenberger, K.J., Storlazzi, C.D., Cheriton, O.M., McPhee-Shaw, E. E., 2016. Variability of the internal tide on the southern Monterey Bay continental shelf and associated bottom boundary layer sediment transport. Cont. Shelf Res. 120, 68—81, http://dx.doi.org/10.1016/j.csr.2016.03.016.

Roux, J.P.l., 1994. Net sediment transport patterns inferred from grain-size trends, based upon definition of "transport vectors" — comment. Sediment. Geol. 90 (1—2), 153—156, http://dx.doi.org/10.1016/0037-0738(94)90022-1.

Saito, Y., Yang, Z., Hori, K., 2001. The Huanghe (Yellow River) and Changjiang (Yangtze River) deltas: a review on their characteristics, evolution and sediment discharge during the Holocene. Geomorphology 41 (2—3), 219—231, http://dx.doi.org/10.1016/S0169-555X(01)00118-0.

Shen, H., 1986. A model of genesis of the relict sediment on the East China Sea shelf. Acta Oceanol. Sin. 5 (3), 437—446, http://www.cnki.com.cn/Article/CJFDTotal-SEAE198603013.htm.

Shepard, F.P., 1954. Nomenclature based on sand-silt-clay ratios. J. Sediment. Res. 24 (3), 151—158, http://dx.doi.org/10.1306/D4269774-2B26-11D7-8648000102C1865D.

Sternberg, R.W., Larsen, L.H., Miao, Y.T., 1985. Tidally driven sediment transport on the East China Sea continental shelf. Cont. Shelf Res. 4 (1—2), 105—120, http://dx.doi.org/10.1016/0278-4343(85)90024-X.

Su, C.-C., Huh, C.-A., 2002. ^{210}Pb, ^{137}Cs and ^{239,240}Pu in East China Sea sediments: sources, pathways and budgets of sediments and radionuclides. Mar. Geol. 183 (1—4), 163—178, http://dx.doi.org/10.1016/S0025-3227(02)00165-2.

Su, J.L., 2001. A review of circulation dynamics of the coastal oceans near China. Acta Oceanol. Sin. 23 (4), 1—16, (in Chinese), http://dx.doi.org/10.3321/j.issn:0253-4193.2001.04.001.

Wang, L., Li, G., Gao, F., Liu, L., Liu, Y., Dada, O.A., 2014. Sediment records of environmental changes in the south end of the Zhejiang-Fujian coastal mud area during the past 100 years. Chin. J. Oceanol. Limnol. 32 (4), 899—908.

Wang, Z.-B., Yang, S.-Y., Zhang, Z.-X., Ri-Hui, L.I., Wang, H., Lan, X.-H., 2012. The grain size compositions of the surface sediments in the East China Sea: indication for sedimentary environments. Oceanol. Limnol. Sin. 43 (6), 1039—1049, http://dx.doi.org/10.1007/s11783-011-0280-z.

Xia, P., Meng, X., Yin, P., Cao, Z., Wang, X., 2011. Eighty-year sedimentary record of heavy metal inputs in the intertidal sediments from the Nanliu River estuary, Beibu Gulf of South China Sea. Environ. Pollut. 159 (1), 92—99, http://dx.doi.org/10.1016/j.envpol.2010.09.014.

Xu, G., Liu, J., Liu, S., Wang, Z., Hu, G., Kong, X., 2016. Modern muddy deposit along the Zhejiang coast in the East China Sea: response to large-scale human projects. Cont. Shelf Res. 130, 68—78, http://dx.doi.org/10.1016/j.csr.2016.10.007.

Xu, K., Li, A., Liu, J.P., Milliman, J.D., Yang, Z., Liu, C.-S., Kao, S.-J., Wan, S., Xu, F., 2012. Provenance, structure, and formation of the mud wedge along inner continental shelf of the East China Sea: a synthesis of the Yangtze dispersal system. Mar. Geol. 291—294, 176—191, http://dx.doi.org/10.1016/j.margeo.2011.06.003.

Xu, K., Milliman, J.D., Li, A., Liu, J.P., Kao, S.-J., Wan, S., 2009. Yangtze- and Taiwan-derived sediments on the inner shelf of East China Sea. Cont. Shelf Res. 29 (18), 2240—2256, http://dx.doi.org/10.1016/j.csr.2009.08.017.

Yamashita, S., Naruse, H., Nakajo, T., 2018. Reconstruction of sediment-transport pathways on a modern microtidal coast by a new grain-size trend analysis method. Prog. Earth Planetary Sci. 5 (1), 18 pp., http://dx.doi.org/10.1186/s40645-018-0166-9.

Yanagi, T., Takahashi, S., Hoshika, A., Tanimoto, T., 1996. Seasonal variation in the transport of suspended matter in the East China Sea. J. Oceanogr. 52 (5), 539—552, http://dx.doi.org/10.1007/bf02238320.

Yuan, D., Zhu, J., Li, C., Hu, D., 2008. Cross-shelf circulation in the Yellow and East China Seas indicated by MODIS satellite observations. J. Mar. Syst. 70 (1—2), 134—149, http://dx.doi.org/10.1016/j.jmarsys.2007.04.002.

Zhang, C., Hong, H., Hu, C., Shang, S., 2011. Evolution of a coastal upwelling event during summer 2004 in the southern Taiwan Strait. Acta Oceanol. Sin. 30 (1), 1—6, http://dx.doi.org/10.1007/s13131-011-0084-9.

Zhang, Q., Liu, H., Qin, S., Yang, D., Liu, Z., 2014. The study on seasonal characteristics of water masses in the western East China Sea shelf area. Acta Oceanol. Sin. 33 (11), 64—74, http://dx.doi.org/10.1007/s13131-014-0556-9.

Zhang, W., Zheng, J., Ji, X., Hoitink, A.J.F., van der Vegt, M., Zhu, Y., 2013. Surficial sediment distribution and the associated net sediment transport pattern in the Pearl River Estuary, South China. Cont. Shelf Res. 61—62, 41—51, http://dx.doi.org/10.1016/j.csr.2013.04.011.

Zheng, Y., Huang, W., 1993. A preliminary analysis on the characteristics of the Kuroshio Frontal Eddy in the East China Sea in spring. Chin. J. Oceanol. Limnol. 11 (3), 276—284, http://dx.doi.org/10.1007/BF02850861.